Insertion of Isocyanides into Group 4 Metal−Carbon and Metal−Nitrogen Bonds. Syntheses and DFT Calculations

Ana M. Martins,* José R. Ascenso, Cristina G. de Azevedo, Alberto R. Dias, M. Teresa Duarte, João F. da Silva, Luís F. Veiros, and Sandra S. Rodrigues

Centro de Química Estrutural, Instituto Superior Técnico, Avenida Rovisco Pais no. 1, 1049-001 Lisboa, Portugal

Received March 19, 2003

The reactions of [Ti(η^5-Ind)(NMe_2)$_2$Me], [Ti(η^5-Ind)(NMe_2)Cl_2], and [Zr(η^5-Ind)(NMe_2)$_2$Cl] with 2,6-dimethylphenyl isocyanide (CN(2,6-Me_2Ph)) and *tert*-butyl isocyanide (CN-*t*-Bu) have been investigated. For the first complex, insertion occurs exclusively into the Ti−C bond to give [Ti(η^5-Ind)(NMe_2)$_2${C(Me)=N-*t*-Bu}] (**1**), which, according to DFT results, is due to the weakness of the Ti−CH_3 bond when compared to Ti−NR_2. [Ti(η^5-Ind)(NMe_2)Cl_2] was found to react with 1 equiv of CN(2,6-Me_2Ph) to yield [Ti(η^5-Ind){C(NMe_2)=N(2,6-Me_2Ph)}Cl_2] (**2**). Two equivalents of 2,6-dimethylphenyl isocyanide reacts with [Zr(η^5-Ind)(NMe_2)$_2$Cl] to give the double insertion compound [Zr(η^5-Ind){C(NMe_2)=N(2,6-Me_2Ph)}$_2$Cl] (**3**). The same reaction performed with CN-*t*-Bu proceeds slowly and enabled the characterization, by NMR, of [Zr(η^5-Ind)(NMe_2){C(NMe_2)=N-*t*-Bu}Cl] (**4**) and [Zr(η^5-Ind){C(NMe_2)=N-*t*-Bu}$_2$Cl] (**5**). The molecular structures of **2** and **3** have been determined by X-ray diffraction. DFT calculations of the insertion of CNH in the zirconium nitrogen bonds of [Zr(η^5-Ind)(NR_2)$_2$Cl] (R = H, Me) have been performed and show that the progressive stability of the insertion products accounts for the experimentally found double insertion product.

Introduction

Due to its implication in organic and organometallic syntheses and also to its role in homogeneous catalysis, the insertion of unsaturated reagents into M−C bonds of transition metal complexes is one of the most important chemical reactions. Among a great diversity of substrates, the insertion of isocyanides was subject to extensive studies.[1] The participation of the resulting iminoacyl ligands in several chemical transformations is very wide, including reactions such as isomerization into vinylamido and η^3-azallyl,[2] C−C coupling leading to imines[3] and enediamido or enamidolate ligands,[4] and intramolecular coupling with alkynes.[5] The relevance of transition metal−carbon bonds stimulated the synthesis of transition metal−amido complexes aiming at the comparison between the reactivity of metal−carbon and metal−nitrogen bonds. This goal was largely frustrated by the lack of reactivity of many metal−amido compounds toward insertion, and few examples of metal−iminocarbamoyl derivatives, formed by insertion of isocyanides into metal−amido bonds, have been reported.[6] These reactions are important in the general context of the amination of organic substrates for which titanium and zirconium imido complexes proved to be useful catalysts.[7]

In this paper we report the insertion of CN(2,6-Me_2Ph) and CN-*t*-Bu into metal−carbon and metal−nitrogen bonds of titanium and zirconium indenyl amido complexes previously reported.[8] The reaction mechanism for the isocyanide insertion into Zr−N bonds was studied by ab initio[9] and DFT[10] calculations, and the

* Corresponding author. E-mail: ana.martins@ist.utl.pt.

(1) (a) Pohlki, F.; Doye S. *Chem. Soc. Rev.* **2003**, *32*, 104. (b) Galindo, A.; Gómez, M.; Gómez-Sal, P.; Martín, A.; del Rio, D.; Sánchez, F. *Organometallics* **2002**, *21*, 293. (c) Thorn, M. G.; Fanwick, P. E; Rothwell, I. P. *Organometallics* **1999**, *18*, 4442. (d) Alcalde, M. I.; Gómez-Sal, M. P.; Royo, P. *Organometallics* **1999**, *18*, 546. (e) Rietveld, M. H. P.; Hagen, H.; van de Water, L.; Grove, D. M.; Kooijman, H.; Veldman, N.; Spek, A. L.; van Koten, G. *Organometallics* **1997**, *16*, 168. (f) Scott, M. J.; Lippard, S. J. *Organometallics* **1997**, *16*, 5857. (g) Durfee, L. D.; Rothwell, I. P. *Chem. Rev.* **1988**, *88*, 1059.

(2) (a) Amador, U.; Daff, P. J.; Poveda, M. L.; Ruiz, C.; Carmona, E. *J. Chem. Soc., Dalton Trans.* **1997**, 3145. (b) Filippou, A. C.; Grünleitner, W.; Völk, C.; Kiprof, P. *J. Organomet. Chem.* **1991**, *413*, 181. (c) Beshouri, S. M.; Chebi, D. E.; Fanwick, P. E.; Rothwell, I. P. *Organometallics* **1990**, *9*, 2375.

(3) (a) Bashall, A.; Collier, P. E.; Gade, L. H.; McPartlin, M.; Mountford, P.; Pugh, S. M.; Radogevic, S.; Schubart, M.; Scowen, I. J.; Trösch, D. J. M. *Organometallics* **2000**, *19*, 4784. (b) Cadierno, V.; Zablocka, M.; Donnadieu, B.; Igau, A.; Majoral, J.-P.; Skowronska, A. *J. Am. Chem. Soc.* **1999**, *121*, 11086.

(4) (a) Greidanus-Strom, G.; Carter, C. A. G.; Stryker, J. M. *Organometallics* **2002**, *21*, 1011. (b) Ong, T.-G.; Wood, D.; Yap, G. P. A.; Richeson, D. S. *Organometallics* **2002**, *21*, 1. (c) Chamberlain, L. R.; Durfee, L. D.; Fanwick, P. E.; Kobriger, L. M.; Latesky, S. L.; McMullen, A. K.; Steffey, B. D.; Rothwell, I. P.; Folting, K.; Huffman, J. C. *J. Am. Chem. Soc.* **1987**, *109*, 6068.

(5) (a) Venne-Dunker, S.; Ahlers, W.; Erker, G.; Fröhlich, R. *Eur. J. Inorg. Chem.* **2000**, 1671. (b) Curtis, M. D.; Real, J.; Hirpo, W.; Butler, W. M. *Organometallics* **1990**, *9*, 66.

(6) (a) Alcalde, M. I.; Gómez-Sal, M. P.; Royo, P. *Organometallics* **2001**, *20*, 4623. (b) Sánchez-Nieves, J.; Royo, P.; Pellinghlli, M. A.; Tiripicchio, A. *Organometallics* **2000**, *19*, 3161. (c) Thirupathi, N; Yap, G. P. A.; Richeson, D. S. *Organometallics* **2000**, *19*, 2573. (d) Broder, C. K.; Goeta, A. E.; Howard, J. A. K.; Hughes, A. K.; Johnson, A. L.; Malget, J. M.; Wade, K. *J. Chem. Soc., Dalton Trans.* **2000**, 3526. (e) Wu, Z.; Diminnie, J. B.; Xue, Z. *Organometallics* **1999**, *18*, 8, 1002. (f) Galakhov, M.; Gómez-Sal, M. P.; Martín, A.; Mena, M.; Yélamos, C. *Eur. J. Inorg. Chem.* **1998**, 1319. (g) Zanella, P.; Brianese, N.; Casellato, U.; Ossola, F.; Porchia, M.; Rossetto, G.; Graziani, R. *J. Chem. Soc., Dalton Trans.* **1987**, 2039. (h) Chisholm, M. H.; Hammond, C. E.; Ho, D.; Huffman, J. C. *J. Am. Chem. Soc.* **1986**, *108*, 7860.

(7) (a) Haak, E.; Bytschkov, I.; Doye, S. *Angew. Chem., Int. Ed.* **1999**, *38*, 3389. (b) Zuckerman, R. L.; Krska, S. W.; Bergman, R. G. *J. Am. Chem. Soc.* **2000**, *122*, 753. (c) Fairfax, D.; Stein, M.; Livinghouse, T.; Jensen, M. *Organometallics* **1997**, *16*, 1523. (d) Cao, C.; Ciszewski, J. T.; Odom, A. L. *Organometallics* **2001**, *20*, 5011; *Organometallics* **2002**, *21*, 5148.

10.1021/om030211n CCC: $25.00
Publication on Web 09/06/2003

results were compared with the NMR experimental findings of *tert*-butylisocyanide insertion in $Zr-NMe_2$ bonds.

Results and Discussion

Chemical Studies. Insertion into M−C Bonds. The reaction of equimolar amounts of CN-*t*-Bu and [Ti(η^5-Ind)$(NMe_2)_2$Me] led systematically to the formation of product mixtures. ^{1}H NMR spectra of the reaction's crude showed broad bands, suggestive of the formation of polymeric and/or paramagnetic aggregates, which were not possible to identify. The reaction was then performed in a NMR tube and followed by ^{1}H and ^{13}C{^{1}H} NMR spectroscopy. The insertion process is instantaneous. In fact, immediately after the addition of the reagents, a new set of signals, compatible with the formation of [Ti(η^5-Ind)$(NMe_2)_2${C(Me)=N-*t*-Bu}], **1**, appeared. The chemical shifts of the methyl group presented in the carbon (δ 20.5 ppm) and proton (δ 2.32 ppm) spectra are indicative of the insertion of *tert*-butyl isocyanide into the $Ti-CH_3$ bond. Strong evidence of the coordination of the iminoacyl ligand is the shift to lower field of the R*C*=NR′ atom (δ 240.9 ppm), as observed in other compounds such as [ZrCp(ArO)(η^2-C(CH_2Ph)N-*t*-Bu)(CH_2Ph)] (ArO = 2,3,5,6-Ph_4C_6HO; 4,6-*t*-Bu_2-2-PhC_6H_2O) (δ 242−244 ppm),[11] and [Zr{(^{i}PrNH)C$(N^iPr)_2\}_2(CH_2Ph)$}{C(CH_2Ph)N(2,6-Me_2Ph)}] (δ 252.86 ppm).[4b] This resonance is typical of dihapto ligands, very commonly found in group 4 metal complexes. In addition, the NMe_2 proton and carbon chemical shifts in **1** do not suffer any significant modification, denoting that the insertion in the Ti−N bonds did not take place. The indenyl ligand resonances consist of three multiplets between δ 6 and 7.5 ppm. The four protons of the benzene ring give rise to two multiplets (δ 7.21 and 6.75 ppm), and the three protons of the five-membered ring appear together as a multiplet at δ 6.18 ppm. Spin saturation transfer and NOEDIFF experiments are suggestive of a fluxional process that equilibrates the two halves of the indenyl ligand. Saturation of the *t*-Bu singlet, at room temperature, showed the existence of a similar NOE between these protons and both H_2/H_3 of the indenyl (see indenyl label). The rotation of the η^2-coordinated iminoacyl ligand is a fluxional process often observed in solution[2a,12] and accounts for the NMR data.

Although the reaction proceeds instantaneously, the conversion of [Ti(η^5-Ind)$(NMe_2)_2$Me] is not complete when both reagents are mixed in stoichiometric quantities. The addition of an excess of isocyanide displaces the reaction toward the formation of **1** and enables the quantitative conversion of [Ti(η^5-Ind)$(NMe_2)_2$Me] in [Ti(η^5-Ind)$(NMe_2)_2${C(Me)=N-*t*-Bu}], which, in these conditions, is unstable. Successive insertion reactions, either in the Ti−iminoacyl or the $Ti-NMe_2$ bonds, or intramolecular rearrangements involving the iminoacyl and amido ligands may occur and be responsible for the modifications observed in the proton spectra;[13] however, except for a set of signals attributable to indene, we were not able to assign them. The elimination of indene from titanium and zirconium indenyl bis(dimethylamido) compounds has previously been reported and reflects the anionic character of the indenyl ligand in this class of complexes.[8a,14]

The reactions of CN-*t*-Bu with [Ti(η^5-Ind)$(NMe_2)Me_2$] and [Zr(η^5-Ind)$(NMe_2)_2$Me] led to mixtures that were not possible to characterize by NMR.

Insertion into M−N Bonds. The insertion of CN-(2,6-Me_2Ph) into the titanium−nitrogen bond of [Ti(η^5-Ind)$(NMe_2)Cl_2$] led to the synthesis of [Ti(η^5-Ind)-{C(NMe_2)=N(2,6-Me_2Ph)}Cl_2], **2**, which was isolated in 86% yield as dark red crystals. The NMR spectra of **2** show two inequivalent methyl resonances for the NMe_2 moiety, as a result of hindered rotation around the carbon−nitrogen bond. This suggests the conjugation of the C=N(2,6-Me_2Ph) double bond with the NMe_2 lone pair, resulting in delocalized partial multiple bonds through the (2,6-Me_2Ph)N=C=NMe_2 frame. An NOE difference spectrum enabled the assignment of the methyl resonances since the interaction between the *endo* NMe_2 methyl (see iminocarbamoyl label) and the xylyl methyl groups gave a positive NOE peak at δ 2.68 ppm when the resonance at δ 2.01 ppm (2,6-(CH_3)$_2$Ph) was irradiated. The observation of a unique resonance for the methyl xylyl groups is consistent with the free rotation of the ring around the C−N bond. The quaternary carbon of the iminocarbamoyl ligand is, as expected, observed at low field (δ 199.5 ppm) and suggestive of a dihapto coordination. The indenyl NMR resonances show a pattern compatible with an average C_s symmetry structure, implying the rotation of the iminocarbamoyl ligand around its bond to the metal. Variable-temperature ^{1}H NMR experiments were performed. In d_8-toluene, the rotation of the iminocarbamoyl ligand is fast until 193 K since no changes have been observed in the proton spectra. When the temperature of a solution of **2** in C_6D_5Br was raised to 373 K, the NMe_2 signals did not suffer any modification. However, above this temperature, a small peak, which gradually increased in intensity until 413 K, began to appear between the resonances of the two methyl groups, at δ 3.21 ppm. It was not possible to achieve the coalescence temperature, which is higher than 413 K. This temperature is indicative of a considerably high energy barrier for the rotation around the C=NMe_2 bond in comparison to the values reported for organic compounds such as amides, amidine, or enamines, for which those values range from 50 to 90 kJ mol^{-1}.

The insertion of xylyl isocyanide in both metal−dimethylamido bonds of [M(η^5-Ind)$(NMe_2)_2$Cl] (M = Ti, Zr) was exclusively observed for the zirconium deriva-

(8) (a) Ascenso, J. R.; Azevedo, C. G.; Correia, M. J.; Dias, A. R.; Duarte, M. T.; Silva, J. L. F.; Gomes, P. T.; Lourenço, F.; Martins, A. M.; Rodrigues, S. S. *J. Organomet. Chem.* **2001**, *632*, 58−66. (b) Martins, A. M.; Ascenso, J. R.; Azevedo, C. G.; Calhorda, M. J.; Dias, A. R.; Rodrigues, S. S.; Toupet, L.; de Leonardis, P.; Veiros, L. F. *J. Chem. Soc., Dalton Trans.* **2000**, 4332−4338.

(9) Hehre, W. J.; Radom, L.; Schleyer, P. v. R.; Pople, J. A. *Ab Initio Molecular Orbital Theory*; John Wiley & Sons: New York, 1986.

(10) Parr, R. G.; Yang, W. *Density Functional Theory of Atoms and Molecules*; Oxford University Press: New York, 1989.

(11) Thorn, M. G.; Lee, J.; Fanwick, P. E.; Rothwell, I. P. *J. Chem. Soc., Dalton Trans.* **2002**, 3398.

(12) Castro, A.; Galakhov, M.V.; Gómez, M.; Gómez-Sal, M. P.; Martín, A.; Sánchez, F. *J. Organomet. Chem.* **2000**, *595*, 36.

(13) (a) Castro, A.; Galakhov, M. V.; Gómez, M.; Gómez-Sal, M. P.; Martín, A.; Sánchez, F.; Velasco, P. *Eur. J. Inorg. Chem.* **2000**, 2047. (b) Galakhov, M.; Gómez, M.; Jiménez, G.; Royo, P.; Pellinghelli, M. A.; Tiripicchio, A. *Organometallics* **1995**, *14*, 2843.

(14) (a) Diamond, G. M.; Jordan, R. F.; Peterson, J. L. *Organometallics* **1996**, *15*, 4030. (b) Diamond, G. M.; Jordan, R. F.; Peterson, J. L. *J. Am. Chem. Soc.* **1996**, *118*, 8024.

Scheme 1

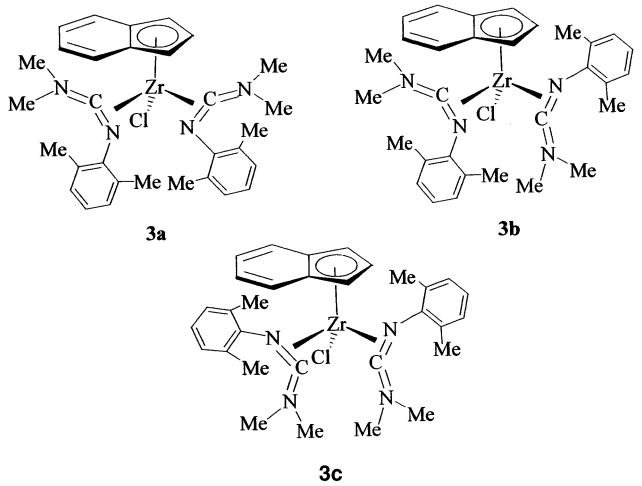

Scheme 2

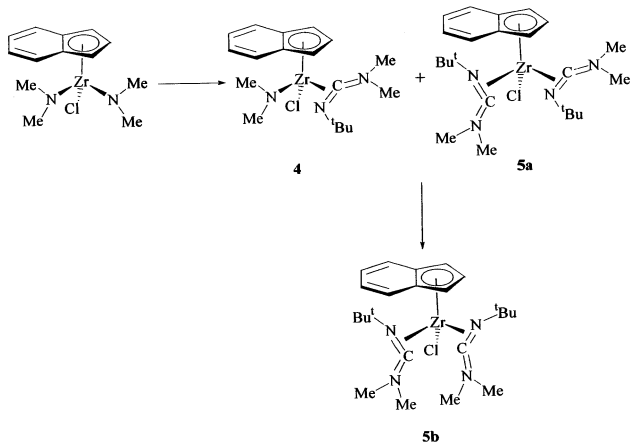

tive. Stereochemical constraints are most probably in the origin of the lack of reactivity of the titanium complex, and similar arguments may justify the absence of insertion of CN-*t*-Bu into the Ti−NMe_2 bonds of [Ti(η^5-Ind)(NMe_2)Cl_2] and [Ti(η^5-Ind)(NMe_2)$_2$Cl]. Complex [Zr(η^5-Ind){C(NMe_2)=N-2,6-Me_2Ph}$_2$Cl], **3**, was obtained in 77% yield as yellow crystals. Considering that the rotation around the Zr−iminocarbamoyl bonds is hindered, three possible isomers, with pseudo-C_s (**3a** and **3c**) and C_1 (**3b**) symmetries, can be drawn for **3**, as depicted in Scheme 1.

The conformer **3c** was the only product obtained when the reaction was left for 24 h at room temperature, as confirmed by NMR and single-crystal X-ray diffraction. As for **2**, the two methyl groups of each NMe_2 fragment in **3** give rise to two singlets, in agreement with the extensive delocalization of electron density through the N−C−N core of the iminocarbamoyl ligands. However, in contrast to what is observed in **2**, hindered rotation around the N−xylyl bonds of **3** leads to the appearance of different resonances for the xylyl methyl groups. As pointed out by the X-ray and theoretical data (see below), this is a stereochemical constraint rather than an electronic effect, resulting from the close location of the two xylyl moieties. The three protons of the indenyl five-membered ring ligand appear at 6.53 ppm as a complex peak. This pattern, previously encountered in other titanium and zirconium indenyl complexes,[8b] is attributed to local magnetic field anisotropy, created by the unsaturated ligands.

The failure to isolate a pure complex from the reaction of [Zr(η^5-Ind)(NMe_2)$_2$Cl] with 1 equiv of CN(2,6-Me_2Ph) led us to the study of the insertion reaction of isocyanides into zirconium−nitrogen bonds by NMR, using as starting materials [Zr(η^5-Ind)(NMe_2)$_2$Cl] and CN-*t*-Bu, and by DFT, using [Zr(η^5-Ind)(NR_2)$_2$Cl] (R = Me or H) and CNH as an isocyanide model.

The insertion of CN-*t*-Bu in the Zr−NMe_2 bonds of [Zr(η^5-Ind)(NMe_2)$_2$Cl] is a slow reaction on the NMR time scale and allowed the identification of all the intermediates. The reaction sequence is depicted in Scheme 2.

The formation of complexes [Zr(η^5-Ind)(NMe_2)-{C(Me_2N)=N-*t*-Bu}Cl], **4**, and [Zr(η^5-Ind){C(Me_2N)=N-*t*-Bu}$_2$Cl], **5a**, is almost simultaneous, either when 1 or 2 equiv of isocyanide is added to [Zr(η^5-Ind)(NMe_2)$_2$-Cl]. The isomerization to **5b** took place very slowly in the NMR tube. Raising the temperature led to the appearance of indene resulting from partial decomposition of the products.

The ^{1}H NMR spectrum at room temperature of the reaction mixture shows two sets of seven resonances attributable to the indenyl ligands of **4** and **5a**. The observation of seven peaks for **4** attests to the existence of a chiral metal center and is compatible with the free rotation around the zirconium−iminocarbamoyl bond. The indenyl pattern shown for **5a** is, as for **4**, consistent with a C_1 symmetry. However, in **5a**, the data imply hindered rotation of the iminocarbamoyl ligands, a result that is mainly due to stereochemical constraints. Surprisingly, for both compounds, the magnetic equivalence of the two methyl groups in each $CNMe_2$ iminocarbamoyl fragment was observed. This is consistent with free rotation around the C−NMe_2 bonds and reflects a reduced multiple-bond character comparing to **2** and **3**. The ^{13}C{^{1}H} spectrum of the reaction mixture shows a great complexity of signals that, except for those corresponding to the quaternary iminocarbamoyl carbons, were impossible to assign. The isomerization to **5b** is readily observed by NMR due to the existence of an average symmetry plane. The indenyl ligand leads to four proton and to five carbon resonances. A gHMBC (^{1}H−^{15}N) heteronuclear correlation performed for **5b** allowed the distinction between the two nitrogen atoms of the iminocarbamoyl ligands that appeared at δ 448 (*t*-Bu*N*C) and 304 ppm (C=*N*Me_2). These values present a dramatic deshielding relative to the free *tert*-butylisocyanide chemical shift, observed at δ −186.5 ppm.[15]

Crystallographic Studies. The molecular structures of complexes **2** and **3** are depicted in Figure 1 and Figure 2, respectively, and selected bond lengths and angles are listed in Tables 1 and 2.

In **2**, the titanium adopts a distorted piano stool geometry, considering the medium point of the C=N(2,6-Me_2Ph) bond ((CN)*) and the C_5 indenyl centroid (C5*) as occupying the bonding positions. The coordination angles C5*−Ti−X (X = Cl, (CN)*) are larger than the Cl−Ti−X angles (X = Cl, (CN)*), and the indenyl plane and that defined by Cl(1), Cl(2), and (CN)* are close to parallel, with an angle of 5.2(7)° between them.

(15) Pflug, J.; Bertulat, A.; Kehr, G.; Fröhlich, R.; Erker, G. *Organometallics* **1999**, *18*, 3818.

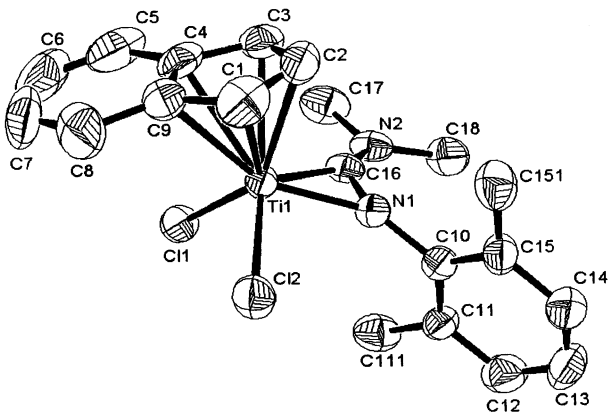

Figure 1. Molecular diagram of **2**. H atoms were omitted for clarity. Ellipsoids were drawn at the 40% probability level with ORTEP3.

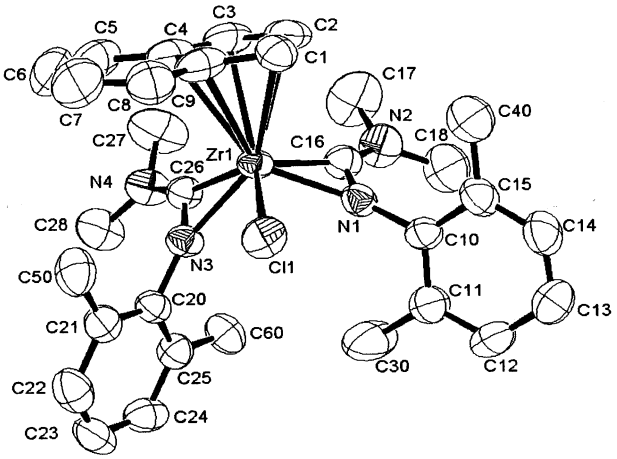

Figure 2. Molecular diagram of one of the molecules of **3** found in the asymmetric unit. H atoms were omitted for clarity. Ellipsoids were drawn at the 40% probability level with ORTEP3.

The general features of the molecular structure concerning distances between the metal and the indenyl carbon atoms and the Ti−Cl bonds are similar to those reported for other Ti(IV) half-sandwich complexes.[8b,16] The iminocarbamoyl ligand shows a η^2-coordination, with Ti(1)−C(16) and Ti(1)−N(1) distances (2.023(5) and 1.982(4) Å) comparable to other Ti−C(sp^2) and Ti−N(sp^2) bond lengths, respectively.[6f,17] Consistent with the NMR spectra, the distances between C(16) and the two nitrogen atoms (1.308(6) and 1.294(5) Å) reveal double-bond character. The iminocarbamoyl fragment (C(17)−N(2)−C(18)−C(16)−N(1)) is planar (rmsd of 0.019(4) Å), with a relative orientation to the indenyl ring given by the angle C5*−Ti−(CN)* of 119.2(6)°. This arrangement points the N(2), C(16), and N(1) p orbitals in an adequate position to extend the π system through the three atoms. The xylyl ring defines with the iminocarbamoyl moiety an angle of 70.8(6)°, a position that minimizes the stereochemical hindrance between the *endo* NMe_2 methyl (C(18)) and the xylyl methyl (C(111)) that are directed toward the same region (C···C; H···H distances of 3.55 and 2.18 Å, respectively). This geometry is also characterized by the torsion angles C5*−Ti−(CN)*−C(10), C(11)−C(10)−N(1)−C(16), and C(15)−C(10)−N1−C(16) of 117.5(6)°, −59.5(6)°, and 124.4(6)°, respectively.

Table 1. Selected Bond Lengths (Å) and Angles (deg) for 2

Distances, Å	
Ti(1)−Cl(1)	2.293(2)
Ti(1)−Cl(2)	2.347(2)
Ti(1)−N(1)	1.982(4)
Ti(1)−C(16)	2.023(5)
N(2)−C(16)	1.308(6)
N(2)−C(17)	1.466(6)
N(2)−C(18)	1.461(6)
N(1)−C(16)	1.294(5)
N(1)−C(10)	1.427(5)
Angles, deg	
C(16)−Ti(1)−N(1)	37.7(2)
C(16)−Ti(1)−Cl(1)	90.9(1)
C(16)−Ti(1)−Cl(2)	123.0(1)
Cl(1)−Ti(1)−Cl(2)	98.06(6)
N(1)−Ti(1)−Cl(1)	111.8(1)
N(1)−Ti(1)−Cl(2)	88.2(1)
Ti(1)−N(1)−C(10)	149.6(3)
Ti(1)−N(1)−C(16)	72.9(3)
C(16)−N(1)−C(10)	134.3(4)
Ti(1)−C(16)−N(2)	155.9(4)
Ti(1)−C(16)−N(1)	69.4(2)
N(1)−C(16)−N(2)	134.6(4)
C(16)−N(2)−C(18)	124.2(4)
C(16)−N(2)−C(17)	120.0(4)
C(18)−N(2)−C(17)	115.6(4)
Cl(1)−Ti(1)−(C(16)−N(1))*	101.8(6)
Cl(2)−Ti(1)−(C(16)−N(1))*	106.1(6)
Cl(1)−Ti(1)−C_5*	115.1(6)
Cl(2)−Ti(1)−C_5*	113.8(6)
(C(16)−N(1))*−Ti(1)−C_5*	119.2(6)

In **3**, the zirconium coordination sphere can also be described as a distorted piano stool geometry, with η^2-C=N units and indenyl occupying single coordination sites. The two molecules in the asymmetric unit exhibit identical overall geometry, and only one is discussed.

For this complex, due to the bulkiness of the two iminocarbamoyl ligands, the geometry is more distorted than in **2**. The angles C5*−M−X vary between 106.4(9)° and 119.1(9)°, while the X−M−X angles are 101.2(9)°, 104.8(9)°, and 108.1(9)°. The angle between the indenyl plane and the one defined by (CN)*, Cl(1), and (CN)* is 8.3(4)°. The dihedral angle between the planes of the two iminocarbamoyl ligands (which are planar, with rmsd of 0.04(4) Å) is 63.9(6)°.

The distances between the metal and the indenyl carbon atoms and the Zr−Cl bonds are similar to those reported for other Zr(IV) complexes.[8b,18] Both ligands have similar metal−iminocarbamoyl carbon bond lengths (2.195(8) and 2.222(7) Å), in the range found in zirconium iminoacyl[4b,18] and iminocarbamoyl silyl complexes.[6e] The Zr−N bond lengths (2.135(6) and 2.152(5) Å) are also in agreement with values reported for similar Zr(IV)−N bonds.[19] As found in complex **2** and [Zr{η^2-C(NMe_2)=NAr}$_3$\{η^2-C($Si(SiMe_3)_3$)=NAr}] (Ar = 2,6-Me_2Ph),[6e] the planarity of the ligand and the short N=C (1.295(10); 1.304(10) Å) and C−NMe_2 bonds (1.332(11) and 1.337(10) Å) are indicative of carbon−nitrogen multiple-bond character. Accordingly, the sums

(16) Ready, T. E.; Day, R. O.; Chien, J. C. W.; Rausch, M. D. *Macromolecules* **1993**, *26*, 5822.
(17) Riley, P. N.; Fanwick, P. E.; Rothwell, I. P. *J. Chem. Soc., Chem. Commun.* **1997**, 1109.
(18) Segerer, U.; Blaurock, S.; Sieler, J.; Hey-Hawkins, E. *J. Organomet. Chem.* **2000**, *608*, 21.
(19) Chisholm, M. H.; Hammond, C. E.; Huffman, J. C. *Polyhedron* **2002**, *7*, 2515.

Table 2. Selected Bond Lengths (Å) and Angles (deg) for One of the Molecules Present in the Asymmetric Unit for 3

Distances, Å	
Zr(1)−N(1)	2.135(6)
Zr(1)−N(3)	2.152(5)
Zr(1)−C(16)	2.195(8)
Zr(1)−C(26)	2.222(7)
Zr(1)−Cl(1)	2.538(2)
N(3)−C(26)	1.304(10)
N(3)−C(20)	1.430(9)
N(4)−C(26)	1.337(10)
N(4)−C(27)	1.473(12)
N(4)−C(28)	1.405(12)
N(1)−C(16)	1.295(10)
N(1)−C(10)	1.440(11)
N(2)−C(16)	1.332(11)
N(2)−C(17)	1.465(14)
N(2)−C(18)	1.459(14)
Angles, deg	
N(1)−Zr(1)−C(16)	34.8(3)
C(16)−Zr(1)−C(26)	94.2(3)
C(16)−Zr(1)−N(3)	108.8(3)
C(16)−Zr(1)−Cl(1)	118.3(2)
N(3)−Zr(1)−C(26)	34.6(2)
C(26)−Zr(1)−N(1)	114.6(3)
C(26)−Zr(1)−Cl(1)	121.7(2)
Zr(1)−N(1)−C(16)	75.2(5)
Zr(1)−N(3)−C(26)	75.6(4)
C(16)−N(1)−C(10)	132.7(7)
C(26)−N(3)−C(20)	132.7(6)
Zr(1)−C(16)−N(2)	160.7(7)
Zr(1)−C(26)−N(4)	160.2(6)
Zr(1)−C(16)−N(1)	70.1(4)
Zr(1)−C(26)−N(3)	69.7(4)
N(1)−C(16)−N(2)	128.9(8)
N(3)−C(26)−N(4)	129.6(7)
C(16)−N(2)−C(18)	126.5(8)
C(26)−N(4)−C(28)	126.8(7)
C(16)−N(2)−C(17)	117.7(9)
C(26)−N(4)−C(27)	117.8(8)
C(18)−N(2)−C(17)	115.7(8)
C(28)−N(4)−C(27)	115.3(8)
(C(16)−N(1))*−Zr(1)−(C(26)−N(3))*	108.1(9)
(C(26)−N(3))*−Zr(1)−C_5*	119.1(9)
(C(16)−N(1))*−Zr(1)−C_5*	115.2(9)
C_5*−Zr−Cl(1)	106.4(9)
(C(16)−N(1))*−Zr(1)−Cl(1)	101.2(9)
(C(26)−N(3))*−Zr(1)−Cl(1)	104.8(9)
(N(1)−Zr(1)−C(16))−(N(3)−Zr(1)−C(26))	70.2(9)

of the angles around the NMe_2 groups are close to 360° and the ZrCN and NMe_2 units are nearly coplanar with dihedral angles between the planes defined by Zr(1)−C(16)−N(1) and C(17)−N(2)−C(18), and Zr(1)−C(26)−N(3) and C(27)−N(4)−C(28) of 7.6(9)° and 7.8(9)°, respectively. As in the previous complex, the xylyl rings adopt an optimal relative conformation to minimize possible stereochemical interactions, presenting angles of 80.5(9)° and 71.5(9)° with the planes of the iminocarbamoyl to which they are bonded. The two xylyl rings are almost perpendicular to the indenyl (angles of 79.2(9)° and 85.2(9)°) and define an angle of 75.9(9)° relative to each other. This optimal geometry is also characterized by the torsion angles C5*−M−(CN)*−C of 110.4° and −130.1° and N−C−N−C_{xylyl} of 9.5° and 3.3°. Short interactions between the *endo* NMe and Me-xylyl groups, with H···H distances of 2.01 (C(28)−C(60)) and 2.86 Å (C(40)−C(18)) are observed.

Molecular Orbital Studies. The mechanism of isocyanide insertion CNH in the Zr−N bonds of [Zr(η^5-Ind)$(NR_2)_2$Cl] (R = H, Me) was studied by DFT/B3LYP molecular orbital calculations. To evaluate the method's performance in the description of the systems studied, the optimization of the geometries of model complexes, [Ti(η^5-Ind){C(NH_2)=NH}Cl_2] and [Zr(η^5-Ind){C(NH_2)=NH}$_2$Cl], was carried out. The results are presented in Figure 3.

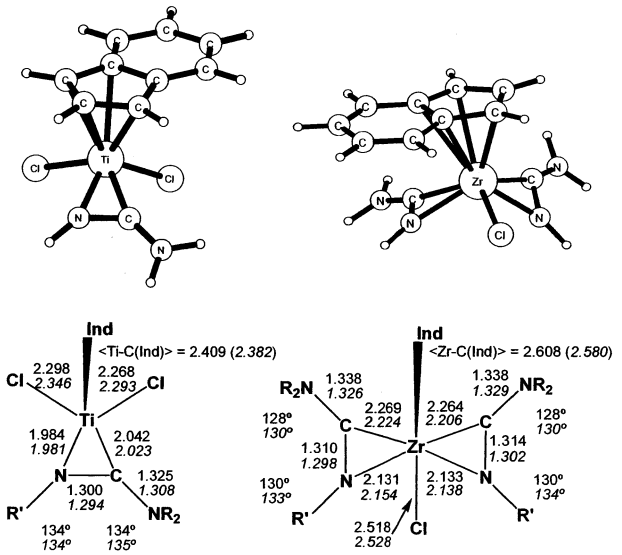

Figure 3. B3LYP optimized geometries of [Ti(η^5-Ind)$(H_2C{=}NH)Cl_2$] (left) and [Zr(η^5-Ind)$(H_2C{=}NH)_2$Cl] (right) with the more relevant distances (Å) and angles (deg) (bottom). The experimental values are presented in italics (for the Zr species these were taken as the mean of the two independent molecules of the asymmetric unit).

Both complexes have piano stool geometries considering that the iminocarbamoyl ligands occupy one coordination position. The agreement between the calculated and the experimental geometries is very good, as shown by the comparison of bond distances about the metal and the C−N distances in the iminocarbamoyl ligands. In fact, the mean and maximum absolute deviations for these distances are 0.021 and 0.058 Å for the Zr complex and 0.014 and 0.048 Å for the Ti species, respectively. The indenyl coordination mode and the relative orientation of the ligands in each complex are also well described by the model. The indenyl coordinates in a slightly distorted η^5 mode, as shown by the small values of the hinge angle, Ω.[20] The experimental values of Ω are 1° and 4° for the Ti and the Zr complexes, respectively, and the corresponding calculated angles are 6° and 2°. The relative orientation of the indenyl with respect to the other three ligands can be measured by the torsion angles C6*−C5*−M−X, where X = Cl, N, or C and C5* and C6* represent the centroids of the C_5 and the C_6 rings of the indenyl ligand, respectively. Thus, for the Ti complex, the benzene moiety of the indenyl ligand lies opposite the iminocarbamoyl and closer to one of the chloride ligands with C6*−C5*−Ti−Cl angles of 24° and 88° (experimental) and 22° and 92° (calculated). In the Zr species the indenyl benzene ring lies over one of the C(NR_2)NR′ ligands, and the C6*−C5*−Zr−Cl values are 75° (calculated) and 62° (experimental, mean of the two independent molecules of the asymmetric unit). The good performance of the

(20) Faller, J. W.; Crabtree, R. H.; Habib, A. *Organometallics* **1985**, *4*, 929.

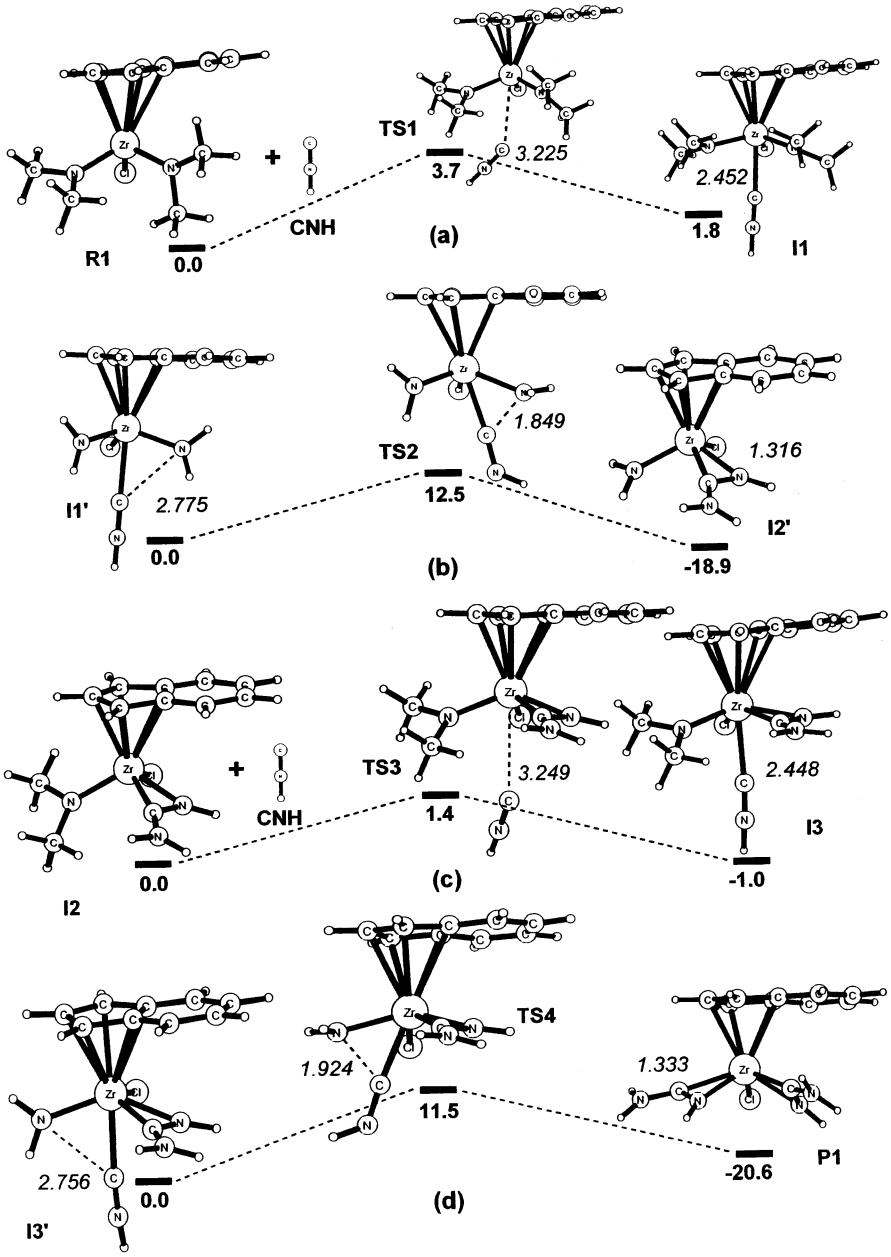

Figure 4. Calculated mechanism (B3LYP) for the consecutive addition (a and c) and insertion (b and d) of one isocyanide molecule, CNR′, into each Zr−N bond of [Zr(η^5-Ind)$(NR_2)_2$Cl]. The relative energies (kcal/mol, bold) and more relevant distances (Å, italic) are presented for each step.

theoretical method in the description of the relative orientation of the ligands in complexes **2** and **3** is especially relevant considering that bulky substituents in the real molecules (R = Me and R′ = 2,6-Me_2Ph) were replaced by hydrogen atoms in the calculations (R = R′ = H) and points out that the major factors determining the geometry around the metals are of electronic rather than stereochemical nature. This is further reinforced by the calculated N−C−N and C−N−R′ angles, which, despite the simplicity of the models, present a mean and maximum absolute deviation of 2° and 4° with respect to the experimental values observed for the two complexes.

The insertion of CNH in the Zr−N bonds of [Zr(η^5-Ind)$(NR_2)_2$Cl] (R = Me, H) was explored. The proposed mechanism is presented in Figure 4 and is based on four individual steps representing the addition of each incoming isocyanide in the metal sphere (steps a and c) followed by insertion in a Zr−N bond (steps b and d), forming an addition(a)−insertion(b)−addition(c)−insertion(d) sequence. Figure 4 shows the energy profile for each step and the optimized geometries of the reactants, products, and the corresponding transition states, together with the most relevant structural parameters. Interestingly the indenyl ligand remains essentially η^5-coordinated along the reaction, the maximum Ω value (8°) being found for **I1**.

The models used to calculate the addition steps were [Zr(η^5-Ind)$(NMe_2)_2$Cl] and [Zr(η^5-Ind){η^2-C(NH_2)═NH}-(NMe_2)Cl] because the replacement of NMe_2 by NH_2 led to a false hydrogen interaction between the incoming isonitrile and the hydrogens of the NH_2 ligands (N−H···C−NH) in the corresponding transition states (**TS1** and **TS3**). However, due to computational limita-

tions, both the amido and the isonitrile substituents were replaced by hydrogen atoms (R = R′ = H) in the remaining calculations.

The first step represents the addition of one CNH to [Zr(η^5-Ind)(NMe_2)$_2$Cl], **R1**. The isonitrile approaches the complex opposite the indenyl ligand, passing through a relatively early transition state (**TS1**) with a Zr−C(CNH) distance of 3.225 Å, which leads to a metal-coordinated isonitrile intermediate, [Zr(η^5-Ind)(NMe_2)$_2$-(CNH)Cl], **I1**, with a Zr−C bond length of 2.45 Å. The major geometrical changes on the Zr coordination sphere are the opening of the N−Zr−N and N−Zr−Cl angles, which increase an average of 5° from **R1** to the transition state **TS1** and 10° in the intermediate **I1**. The resulting Zr−C bond is already incipient in the transition state, as shown by the corresponding Wiberg indexes, WI, 0.0776 and 0.3857 in **TS1** and **I1**, respectively.

The second step corresponds to the insertion of the coordinated isocyanide of intermediate **I1′** into one Zr−NH_2 bond, leading to the intermediate [Zr(η^5-Ind)-(NH_2){C(NH_2)═NH}Cl], **I2′**, which contains amido and iminocarbamoyl ligands. The major change associated with this step is the formation of the new C−N bond of HNC−NH_2, as pointed out by the C−N distance variations from 2.78 Å in **I1′** to 1.85 Å in **TS2** and 1.32 Å in **I2′**. A strong C−N interaction is already present in the transition state **TS2**, as emphasized by the Wiberg index (WI = 0.5647) that results in bond formation in **I2′**, with WI{C−N} = 1.3075. Other minor changes associated with this step are the weakening of the Zr−NH_2 and C−NH bonds (d{Zr−N} = 2.02, 2.19, 3.59 Å; WI{Zr−N} = 0.9963, 0.5212, 0.0330, for **I1′**, **TS2**, and **I2′**, respectively; d{C−N} = 1.17, 1.23, 1.32 Å; WI{C−N} = 2.5131, 2.2073, 1.5211, for **I1′**, **TS2**, and **I2′**, respectively) and the strengthening of the Zr−C bond (d{Zr−C} = 2.45, 2.27, 2.28 Å; WI{Zr−C} = 0.3742, 0.5568, 0.5244, for **I1′**, **TS2**, and **I2′**, respectively).

The third step describes the addition of a second isocyanide to [Zr(η^5-Ind)(NMe_2){C(NH_2)═NH}Cl], **I2**. This step is similar to the first one both on geometrical and on electronic grounds, with a stepwise increase of the L−Zr−L angles that vary a mean value of 4° from **I2** to **TS3** and 8° from **I2** to **I3** (L represents the chloride, the amido nitrogen, and the midpoint of the C−N iminocarbamoyl bond). However, contrary to what happened in the first addition step, where an even increase was found for the three L−Zr−L angles, in this case the $C_{(CNR')}$−Zr−iminocarbamoyl angle is that presenting a greater increase, 19°, on going from **I2** to **I3**. An odd widening of the X−Zr−X angles is observed for **I3**, due to the shift of the chloride ligand away from the iminocarbamoyl (Cl−Zr−iminocarbamoyl = 129°) and closer to the amido ligand (Cl−Zr−N = 102°). The Zr−C(CNH) distances in the transition state **TS3** and in the resulting intermediate, **I3**, are 3.25 and 2.45 Å, respectively, and the corresponding Wiberg indexes are 0.0767 and 0.3976, showing that the Zr−CNH bond formed in **I3** is present in the transition state as a weak interaction, in close resemblance to what was obtained for the first addition.

Another aspect of both addition steps is the electronic enrichment of the metal atom due to the addition of CNH, as reflected by the Zr charges (NPA) that vary from 1.69 in **R1** to 1.66 in **I1** and from 1.61 in **I2** to 1.54 in **I3**. Some conclusions can be drawn based on those values. The comparison between the Zr charges in **I1** and **I2** reveals a more electron rich metal in the later species, showing that in this environment an iminocarbamoyl ligand is a better electron donor than NMe_2 and CNH together. Additionally, the comparison of the Zr charges in **R1** and **I2**, which differ uniquely in the replacement of an amido by an iminocarbamoyl ligand, confirms the later ligand as a better electron donor.

The last step of the mechanism is the insertion of the coordinated isonitrile in **I3′** into the remaining Zr−NMe_2 bond, leading to the product **P1**, which has two iminocarbamoyl ligands resulting from the overall insertion of two isonitriles in the Zr−N(amido) bonds of the original diamido complex, **R1**. As for the second step, the major geometrical and electronic changes are again associated with the formation of the C−NR_2 bond. The distance between the two atoms shortens from 2.76 Å in **I3′** to 1.33 Å in **P1** (WI{C−N} = 1.3134), and the interaction is already present in the transition state (**TS4**), with a 1.92 Å bond distance and a 0.5029 Wiberg index.

An interesting aspect of **P1** is the delocalized double-bond character along the N−C−N frame of the iminocarbamoyl ligands (R′$NCNR_2$). This is suggested by the planarity of the R_2NC fragment of the coordinated iminocarbamoyl ligand in the optimized structure of **P1**, with all the R−N−C−N torsion angles below 5°, and further confirmed by the calculated C−N bond lengths (d{R_2N−C} = 1.33, 1.34 Å, and d{C−NR′} = 1.31, 1.32 Å) and Wiberg indices (WI{R_2N−C} = 1.289, 1.313, and WI{C−NR′} = 1.550, 1.512). These values are intermediate between a typical C≡N triple bond (d{C≡N} = 1.180 Å and WI = 2.429, in CNH) and a single C−N bond (d{C−N} = 1.475 Å and WI = 0.989, in NMe_3), denoting, thus a C═N double-bond character in the coordinated iminocarbamoyl.

The energy profile corresponding to the mechanism shows two rather flat addition steps with low activation energies (3.7 and 1.4 kcal/mol, respectively) and small energy variations (1.8 and −1.0 kcal/mol, in the same order), suggesting that the isonitrile additions correspond to a rapid exchange equilibrium. The insertion steps present significantly larger activation energies (12.5 and 11.5 kcal/mol, respectively), reflecting the greater geometrical and electronic transformations occurring in these steps. On the other hand, each isonitrile insertion is noticeably exothermic (ΔE = −18.9 and −20.6 kcal/mol), pointing out that the transformation of an amido/isonitrile complex into an iminocarbamoyl species is a favorable process. The increasing stability of the complexes along the reaction path is directly related with an enhanced metal electronic richness shown by the Zr charges in the reactant, **R1** (1.69), and the product, **P1** (1.50). The overall energy variation should not be directly taken from Figure 4 individual steps given the different models used for the addition and the insertion elementary steps. However, it can be derived from the following equation, where a **R1′** reactant (with NH_2 instead of NMe_2) is used, suggesting a strongly exothermic reaction:

$$[Zr(\eta^5\text{-Ind})(NH_2)_2Cl]\ (\mathbf{R1'}) + 2\ CNH \rightarrow [Zr(\eta^5\text{-Ind})\{C(NH_2)NH\}_2Cl]\ (\mathbf{P1})$$

$$\Delta E = -48.1\ \text{kcal/mol}$$

The experimental observation of a kinetic and a thermodynamic product identified by NMR (see Scheme 2 and its discussion) led us to a comprehensive study of the different product conformers and their interconversion, resulting from the rotation around the indenyl−metal and the iminocarbamoyl−metal bonds. The results are shown in Figure 5, which depicts the transition states and the minima optimized geometries, as well as the relative energies. It should be noticed that the indenyl ligand coordination remains distorted η^5 along the entire path, the maximum Ω value (7°) being found for **TS7**.

Three conformers result from the different relative orientations of the two iminocarbamoyl and the chloride ligands. The iminocarbamoyl ligands may be coordinated in a symmetric fashion, with the NR_2 and NR′ moieties facing each other, leading to a pseudo-C_s symmetric product. In this case, two possibilities arise for the chloride location: between the NR_2 or between the NR′ moieties, leading respectively to **P3** and **P2**, which corresponds to the crystallographic structure obtained for **3**. Alternatively, the iminocarbamoyl ligands can be asymmetrically coordinated, with each NR_2 fragment facing the NR′ moiety of the other ligand. In this case the product **P1** has C_1 symmetry and results directly from the addition/insertion mechanism discussed above. The interconversion mechanism gave rise to a second conformer with C_1 symmetry, **P1′**, which is related to **P1** by the relative orientation of the indenyl and the NR_2CNR' ligands: the indenyl benzene ring lies over one NR_2CNR' in **P1** and over the other in **P1′**.

The first stage of the interconversion mechanism represented in Figure 5 starts with the rotation of one iminocarbamoyl ligand (on the right side of the molecule) in **P3** to give **P1′**. The relaxation of this structure toward a C_1 symmetry is accompanied by the rotation of the indenyl ligand. The conversion to **P2** requires the rotation of the other iminocarbamoyl ligand. However, due to its location below the indenyl benzene ring, the direct rotation of the second iminocarbamoyl ligand (on the left of the molecule) is disfavored by the proximity of the NR_2 moiety and the indenyl. This is overcome through an intermediate step that places the indenyl C_6 ring over the first carbamoyl ligand, generating a second C_1 symmetric conformer, **P1**. The major geometrical change that goes along with the indenyl rotation through the transition state **TS6** can be measured by the C6*−C5*−Zr−Cl torsion angle that varies from 77° in **P1′** to 1° in **TS6** and 80° in **P1**. No electronic or geometric parameter, other than the dihedral angle, suffers a significant variation along this path, meaning that the destabilization associated with **TS6** is essentially due to the stereochemical repulsion between the indenyl and the chloride ligands. The last step is the rotation of the second iminocarbamoyl ligand to give rise to the second pseudo-C_s product, **P2**. The rotation of the iminocarbamoyl ligands goes through the transition sates **TS5** and **TS7**, where the NR_2CNR' ligands coordinate in an "upright" geometry. The associated geometrical changes can be measured by the N−C−Zr−C5* torsion angles, where N and C are the iminocarbamoyl coordinating atoms and C5* the indenyl C_5 ring centroid. Along the two steps, those angles are 100° in **P3**, 158° in **TS5**, 138° in **P1′,** and 80°, 169°, and 142° in **P1**, **TS7**, and **P2**, respectively. The weakening of the Zr−C bonds in the transition states are the major electronic changes in the iminocarbamoyl rotation steps, as pointed out by the corresponding Wiberg indexes (WI = 0.557 in **P3**, 0.545 in **TS5**, and 0.556 in **P1′**; 0.577 in **P1**, 0.522 in **TS7**, and 0.569 in **P2**). This effect is partially compensated by the reinforcement of the Zr−N bonds, for which the corresponding Wiberg indexes rise from 0.548 in **P3** to 0.573 in **TS5** and from 0.581 in **P1** to 0.598 in **TS7**. Nevertheless, this compensation is not enough to overcome the loss of electron density in the metal center due to the weakening of the Zr−C bond, as shown by the metal charges (1.51 in **P3**, 1.54 in **TS5**, and 1.49 in **P1′**; and 1.50 in **P1**, 1.52 in **TS7**, and 1.50 in **P2**). The depletion of electron density is the main reason for the destabilization associated with the transition states.

Another interesting result, based on the NMR observations, is the preferential insersion of an incoming isonitrile into the Ti−C bond rather than in one of the Ti−N bonds of complex $[Ti(\eta^5\text{-Ind})(NMe_2)_2Me]$. In fact, this is a key step in a recently proposed catalytic cicle for the coupling of amines, alkynes, and isocyanides with a Ti catalyst.[21] The behavior of our system was investigated by means of a comparative study of the insertion of a CNH into a Ti−C and a Ti−N bond of the model Ti complex $[Ti(\eta^5\text{-Ind})(NH_2)_2(CH_3)]$ (**R2**), performed at the same level of theory as the one used for the Zr complex discussed above.

The addition of a CNH molecule to $[Ti(\eta^5\text{-Ind})(NH_2)_2(CH_3)]$ is a slightly endothermic reaction ($\Delta E = 6.1$ kcal/mol), yielding the corresponding intermediate, $[Ti(\eta^5\text{-Ind})(NH_2)_2(CH_3)(CNH)]$ (**I4**), similarly to the Zr complex reaction (see Figure 4) and, thus, not deserving any further discussion. The insersion of the CNH ligand into the Ti−C bond of **I4** results in an iminoacyl complex, $[Ti(\eta^5\text{-Ind})(NH_2)_2(CH_3CNH)]$ (**P4**). If, however, the CNH ligand inserts into a Ti−N bond of one NH_2 ligand, an iminocarbamoyl complex is produced, $[Ti(\eta^5\text{-Ind})(NH_2)(CH_3)\{C(NH_2)NH\}]$ (**P5**), in a reaction equivalent to what was discussed for the Zr complex. The energetic profile for these two reactions is depicted in Figure 6, with the optimized geometries of the intervening species and the more relevant geometrical and electronic parameters.

The two reactions presented are completely equivalent to the insertion steps (2 and 4) of the Zr complex reaction. In all cases the M−L (CH_3 or NH_2) bond breaking and the L−CNH bond forming associated with the insersion are already clearly present in the corresponding transition states (**TS8** and **TS9**), as shown by the bond distances and Wiberg indices of Figure 6. From an energetic point of view the two Ti reactions are, however, quite different. In fact, the insersion of the isonitrile ligand into the Ti−C bond is largely more favorable from a kinetic ($E_a = 1.0$ kcal/mol) as well as from a thermodynamic point of view ($\Delta E = -38.2$ kcal/mol) than the insertion of CNH into a Ti−N bond ($E_a = 7.9$ kcal/mol and $\Delta E = -26.6$ kcal/mol), in absolute

(21) Cao, C.; Shi, Y.; Odom, A. L. *J. Am. Chem. Soc.* **2003**, *125*, 2880.

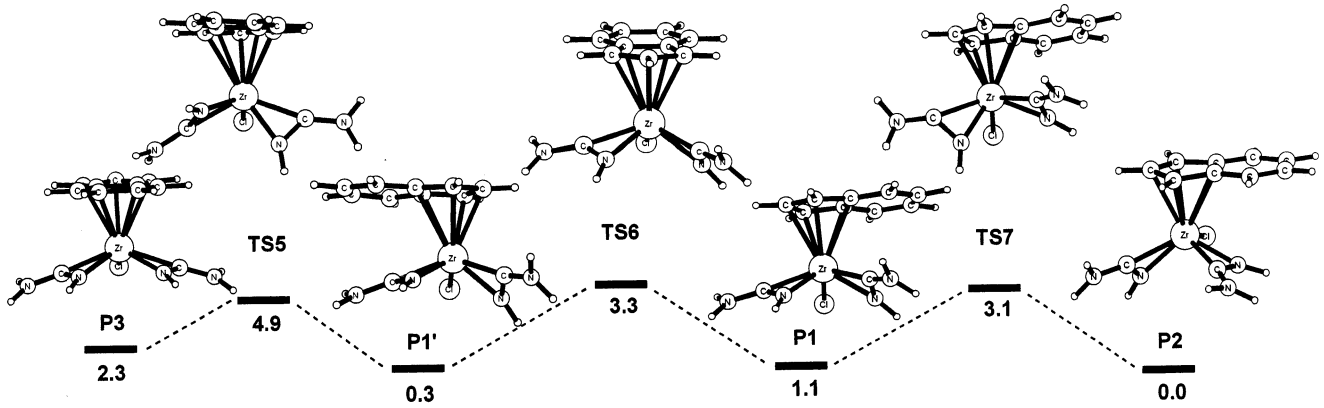

Figure 5. Calculated mechanism (B3LYP) for the interconversion of different [Zr(η^5-Ind)($H_2C{=}NH)_2$Cl] conformers, corresponding to the rotation of the iminocarbamoyl and the indenyl ligands. The relative energies (kcal/mol) are presented.

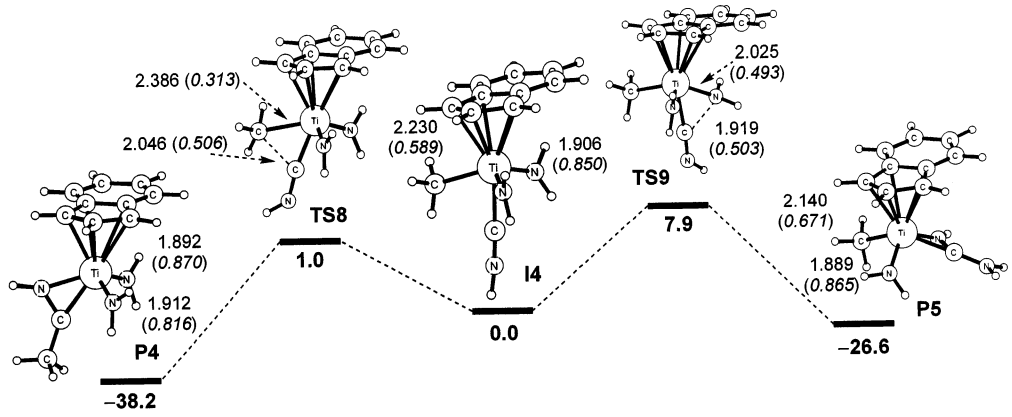

Figure 6. Calculated mechanism (B3LYP) for the insersion of one CNH into a Ti−C (left) or a Ti−N (right) bond of [Ti(η^5-Ind)($NH_2)_2$(CH_3)(CNH)], with the more relevant distances (Å) and the corresponding Wiberg indices (italics). The relative energies (kcal/mol) are presented in bold.

agreement with the NMR data discussed above. This result is caused, essentially, by the difference between the Ti−CH_3 and Ti−NH_2 bond strengths, the former being considerably weaker than the latter (see Figure 6 parameters). Since a weaker bond (Ti−CH_3) is easier to break, the corresponding transition state is easier to reach, and, thus, a faster reaction results. Additionally, a product with two Ti−NH_2 bonds (strong) is more stable by 11.6 kcal/mol than one with one Ti−NH_2 (stronger) and one Ti−CH_3 bond (weaker).

It should be noticed that, given the simplicity of the model complexes used in the calculations, the energy values associated with the mechanisms depicted in Figures 4, 5, and 6 should not be taken in absolute terms, but only their relative values are meaningful. Although the theoretical method employed provides good geometries, at least for the minima (see Figure 3, and its discussion), a good match between the calculated absolute energy values and the real ones cannot be expected since bulky substituents (R = Me, R′ = 2,6-Me_2Ph, *t*-Bu) were replaced by hydrogen atoms in the calculations.

Conclusions

Complex [Ti(η^5-Ind)($NMe_2)_2${C(Me)=N-*t*-Bu}], **1**, was identified by NMR as the product of the insertion of CN-*t*-Bu in the Ti−CH_3 bond of [Ti(η^5-Ind)($NMe_2)_2$Me]. The fact that complex **1** is unstable in the presence of excess isocyanide, leading to the cleavage of the titanium−indenyl bond, prevented its complete characterization. However, the preferencial insertion of an isonitrile into a Ti−C rather than a Ti−N bond was confirmed by DFT calculations. This preference is caused by the relative bond strength of Ti−CH_3 and Ti−NR_2; that is, the insertion in the weaker bond (Ti−CH_3) yields a faster reaction and a more stable final product.

The reactions of CN(2,6-Me_2Ph) with [Ti(η^5-Ind)($NMe_2)Cl_2$] and [Zr(η^5-Ind)($NMe_2)_2$Cl] give [Ti(η^5-Ind){$C(NMe_2){=}N$(2,6-Me_2Ph)}Cl_2], **2**, and [Zr(η^5-Ind)-{$C(NMe_2){=}N$(2,6-Me_2Ph)}$_2$Cl], **3**, by insertion of the isocyanide in the metal−nitrogen bonds. The iminocarbamoyl ligands of **2** and **3** present extensive delocalization of electron density through the N−C−N core.

The insertion of CN-*t*-Bu in the Zr−N bonds of [Zr(η^5-Ind)($NMe_2)_2$Cl] was studied by NMR. The reaction proceeds slowly on the NMR time scale to give [Zr(η^5-Ind){$C(NMe_2){=}$N-*t*-Bu)(NMe_2)Cl], **4**, and [Zr(η^5-Ind){$C(NMe_2){=}$N-*t*-Bu$)_2$Cl], **5**, for which two conformers, corresponding to the kinetic and thermodynamic products, have been characterized.

The experimental results agree with those obtained by DFT calculations of the insertion reaction mechanism. The similarity between the insertion activation energies and the progressive stability of the insertion products accounts for the simultaneous formation of the complexes resulting from one and two isocyanide insertions, even when only 1 equiv of isonitrile is used. The formation of a kinetic product with C_1 symmetry (**5a**)

slowly evolving to a C_s symmetric conformer (**5b**) was endorsed by the calculated interconversion mechanism depicted in Figure 5.

Due to stereochemical constraints that the models do not take in account, the actual energy values are expected to be higher than those calculated. Nevertheless, the calculated energy profiles reflect the reaction mechanism and establish that the reaction is essentially determined by electronic grounds.

Experimental Section

General Procedures. All manipulations were carried out under a dry nitrogen atmosphere with standard Schlenk techniques. Solvents were distilled from the indicated drying agents: pentane (Na), hexane (CaH_2), C_6D_6 (Na), toluene (Na), and ether (Na). CN-*t*-Bu was dried with anhydrous Na_2SO_4 and distilled at room temperature and 10^{-2} mbar. CN(2,6-Me_2Ph) was used as received. Literature methods were used to prepare [Ti(η^5-Ind)(NMe_2)$_2$Me], [Ti(η^5-Ind)(NMe_2)Cl_2], and [Zr(η^5-Ind)(NMe_2)$_2$Cl].[8] NMR spectra were recorded on a Varian Unity 300 instrument at room temperature. ^{1}H and ^{13}C NMR spectra are referenced to solvent. Infrared spectra were obtained with a Perkin-Elmer 577 spectrophotometer. Mass spectra were recorded on a Finnegan MAT System 8200 spectrometer. Elemental analyses were performed on a Fisons Instruments 1108 device.

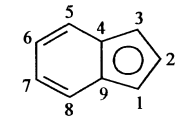

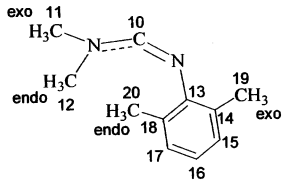

[Ti(η^5-Ind)(NMe_2)$_2${C(Me)=N-*t*-Bu}] (1). *tert*-Butyl isocyanide (0.14 mL, 1.2 mmol) was added to 0.50 mL of an orange C_6D_6 solution of [Ti(η^5-Ind)(NMe_2)$_2$Me] (0.16 g, 0.60 mmol) at room temperature. The reaction was followed by NMR, and the quantitative formation of **1** was observed almost immediately (ca. 4−5 min). After 15 min new unidentifiable broad resonances appeared. Signals attributed to indene are also visible in the spectra. ^{1}H NMR (C_6D_6): δ 7.21 (m, $^3J_{H5H6}$ = 6.3, $^4J_{H5H7}$ = 3.0, 2H, H_5, H_8), 6.75 (m, $^3J_{H6H5}$ = 6.3, $^4J_{H6H8}$ = 3.0, 2H, H_6, H_7), 6.18 (m, 3H, H_1, H_2, H_3), 3.12 (s, 12H, N(CH_3)$_2$), 2.32 (s, 3H, CH_3), 0.90 (s, 9H, *t*-Bu). ^{13}C{^{1}H} RMN (C_6D_6): δ 240.9 (Me*C*=N-*t*-Bu), 125.3 (C_4, C_9), 123.4 (C_5, C_8), 122.4 (C_6, C_7), 116.7 (C_2), 98.1 (C_1, C_3), 58.9 (*C*(CH_3)$_3$), 50.8 (N(*C*H_3)$_2$), 30.0 (C(*C*H_3)$_3$), 20.5 (*C*H_3).

[Ti(η^5-Ind){C(NMe_2)=N(2,6-Me_2Ph))Cl_2] (2). A solution of 2,6-Me_2PhNC (0.21 g, 1.59 mmol) in toluene (10 mL) was added to an orange solution of [Ti(η^5-Ind)(NMe_2)Cl_2] (0.44 g, 1.59 mmol) in the same solvent (20 mL) at room temperature. The resulting solution was stirred for 24 h and then evaporated to dryness. Compound **2** was isolated as an orange solid in 86% yield (0.56 g). Dark red crystals were obtained by cooling a toluene solution to −20 °C. ^{1}H NMR (CD_3CN): δ 7.74 (m, $^3J_{H5H6}$ = 6.4, $^4J_{H5H7}$ = 3.1, 2H, H_5, H_8), 7.34 (m, $^3J_{H6H5}$ = 6.4, $^4J_{H6H8}$ = 3.1, 2H, H_6, H_7), 7.04 (br, 3H, H_{15}, H_{16}, H_{17}), 6.98 (d, $^3J_{H1H2}$ = 3.4, 2H, H_1, H_3), 6.40 (t, $^3J_{H2H1}$ = 3.4, 1H, H_2), 3.33 (s, 3H, H_{11}), 2.68 (s, 3H, H_{12}), 2.01 (s, 6H, H_{19}, H_{20}). ^{13}C{^{1}H} NMR (CD_3CN): δ 199.5 (C_{10}), 146.5 (C_{13}), 132.6 (C_{14}, C_{18}), 129.1 (C_4, C_9), 128.6 (C_{15}, C_{17}), 127.6 (C_6, C_7), 127.0 (C_{16}), 126.8 (C_5, C_8), 118.2 (C_2), 109.1 (C_1, C_3), 44.4 (C_{11}), 37.8 C_{12}), 19.0 (C_{19}, C_{20}). IR (KBr, ν): 1670, vs, 1588, w, ($\nu_{C=N}$). MS (EI, *m*/*z*): 408 (M^+), 373 ({M − Cl}$^+$), 293 ({M − (C_9H_7)}$^+$), 233 ({Ti(C_9H_7)-Cl_2}$^+$), 198 ({Ti(C_9H_7)Cl}$^+$), 175 ({C(NMe_2)=N(Me_2Ph)}$^+$), 145 ({C(NMe_2)=NC_6H_3}$^+$), 115 ({C_9H_7}$^+$), 105 ({Me_2Ph}$^+$), 89 ({$CH_3C_6H_3$}$^+$). Anal. Calcd for $C_{20}H_{22}N_2Cl_2Ti$: C, 58.71; H, 5.42; N, 6.85. Found: C, 58.36; H, 5.37; N, 6.61.

[Zr(η^5-Ind){C(Me_2N)=N(2,6-Me_2Ph)}$_2$Cl] (3). A solution of 2,6-Me_2PhNC (0.31 g, 2.38 mmol) in toluene (10 mL) was added to a yellow solution of [Zr(η^5-Ind)(NMe_2)$_2$Cl] (0.39 g, 1.19 mmol) in the same solvent (20 mL) at −30 °C. The resulting solution was stirred and warmed to room temperature for 18 h. After filtration of a white solid precipitate, redisolution in toluene, and reprecipitation at −15 °C, compound **3** was obtained pure as white in 77% yield (0.54 g). Yellow crystals were obtained by cooling a toluene solution to −20 °C. ^{1}H NMR (C_6D_6): δ 7.69 (m, $^3J_{H5H6}$ = 6.3, $^4J_{H5H7}$ = 3.0, 2H, H_5, H_8), 7.03 (m, $^3J_{H6H5}$ = 6.3, $^4J_{H6H8}$ = 3.0, 2H, H_6, H_7), 6.99−6.90 (m, 3H, H_{15}, H_{16}, H_{17}), 6.53 (m, $^3J_{H1H2}$ = 2.4, 3H, H_1, H_2, H_3), 2.84, 2.30, 2.06, 2.02 (s, 12H, H_{11}, H_{12}, H_{19}, H_{20}). ^{13}C{^{1}H} NMR (C_6D_6): δ 205.8 (C_{10}), 152.7 (C_{14}, C_{18}), 147.4 (C_{13}), 131.6, 130.8 (C_{15}, C_{16}, C_{17}), 125.5 (C_4, C_9), 124.3 (C_5, C_8), 123.2 (C_6, C_7), 117.3 (C_2), 96.2 (C_1, C_3), 45.5, 35.9 (C_{11}, C_{12}), 20.0, 19.5 (C_{19}, C_{20}). IR (KBr, ν): 1699, s, 1602, m, ($\nu_{C=N}$). MS (EI, *m*/*z*): 591 (M^+), 476 ({M − (C_9H_7)}$^+$), 417 ({M − [C(NMe_2)=N(Me_2Ph)] + H}$^+$), 370 ({M − (C_9H_7) − ($Me_2C_6H_4$)}$^+$), 346 ({Zr(C_9H_7)[(Me_2N)CN]$_2$}$^+$), 320 ({M − (C_9H_7) − ($Me_2C_6H_4$) − MeCl}$^+$), 311 ({Zr(C_9H_7)[(Me_2N)-CN]Cl}$^+$), 308 ({(Me_2Ph)N(H)C(NMe_2)CN(H)(Me_2Ph)}$^+$), 206 ({Zr(C_9H_7)}$^+$), 176 ({(Me_2N)CH=N(Me_2Ph)}$^+$), 161 ({MeNCH=N(Me_2Ph)}$^+$), 145 ({(Me_2N)C=NPh}$^+$; {NCN(Me_2Ph)}$^+$), 132 ({HCN(Me_2Ph)}$^+$), 115 ({C_9H_7}$^+$), 105 ({ZrN}$^+$), 91 (Zr^+), 44 ({NMe_2}$^+$). Anal. Calcd for $C_{31}H_{37}N_4ClZr$: C, 57.30; H, 6.12; N, 9.11. Found: C, 57.40; H, 6.03; N, 8.99.

[Zr(η^5-Ind)(NMe_2)Cl{C(NMe_2)=N-*t*-Bu}] (4) and [Zr(η^5-Ind)Cl{C(NMe_2)=N-*t*-Bu}$_2$] (5). A 4-fold excess of *tert*-butyl isocyanide (1.34 mL, 11.90 mmol) was added to 25 mL of a yellow solution of [Zr(η^5-Ind)(NMe_2)$_2$Cl] (0.98 g, 2.96 mmol) in toluene, at room temperature. The resulting solution was heated at 45 °C for 15 h and then evaporated to dryness. A dark orange oil was obtained and characterized by NMR (^{1}H, ^{13}C, and ^{15}N) as a mixture of compounds **4** and **5a**. The addition of pentane, hexane, or ether did not allow the separation of the products. However, by stirring the toluene solution for a month at room temperature, it was possible to isolate **5b** in 85% yield (1.25 g). Data for **4**: ^{1}H NMR (C_6D_6): δ 7.63, 6.90−6.70 (m, 4H, H_5, H_6, H_7, H_8), 5.85, 5.81 (m, 2H, H_1, H_3), 5.68 (t, $^3J_{H2H1}$ = 3.0, 1H, H_2), 2.70 (s, 6H, N(CH_3)$_2$)), 2.79 and/or 2.73 (s, 6H, CNMe_2), 1.18 or 1.09 (s, 9H, *t*-Bu). ^{13}C{^{1}H} NMR (C_6D_6): δ 201.7 (C=N). Data for **5a**: ^{1}H NMR (C_6D_6): δ 7.48, 7.28, 7.15, 6.81 (m, 4H, H_5, H_6, H_7, H_8), 6.51, 6.28 (m, 2H, $^3J_{H1/H2}$/$^3J_{H3/H2}$ = 3.0, H_1, H_3), 6.38 (t, $^3J_{H2H1}$ = 3.0, 1H, H_2), 2.79 and/or 2.73 (s, 12H, CNMe_2) 1.18 and/or 1.09 (s, 18H, *t*-Bu). ^{13}C{^{1}H} RMN (C_6D_6): δ 205.4 (C=N). **5b**: ^{1}H NMR (C_6D_6): δ 7.64 (m, $^3J_{H5/H6}$ = 6.9, 2H, H_5, H_8), 6.92 (m, $^3J_{H6/H5}$ = 6.9, 3H, H_2, H_6, H_7), 6.40 (d, $^3J_{H1H2}$ = 3.0, 2H, H_1, H_3), 2.77 (s, 12H, CNMe_2), 1.22 (s, 18H, *t*-Bu). ^{13}C{^{1}H} RMN (C_6D_6): δ 200.3 (C_{10}), 129.3 (C_4, C_9), 125.0 (C_5, C_8), 122.0 (C_6, C_7), 114.6 (C_2), 96.8 (C_1, C_3), 55.0 (*C*(CH_3)$_3$), 44.8 (NMe_2), 32.5 (C(*C*H_3)$_3$). ^{15}N NMR (C_6D_6): δ 448 (C=*N*), 304 (*N*Me_2). IR (C_6D_6): 1685 (s, $\nu_{C=N}$).

Crystal Structure Determination of Compounds 2 and 3. Crystallographic and experimental details of the crystal structure determinations are given in Table 3. Suitable crystals of complexes **2** and **3** were mounted on a capillary under nitrogen. Data were collected at room temperature on an Enraf Nonius MACH3 diffractometer equipped with Mo radiation (λ = 0.71069 Å). Solution and refinement were made using SIR97[22] and SHELXL[23] included in the package of programs WINGX-Version 1.64.03b.[24]

For compound **3** two molecules (exhibiting slight differences in the geometric parameters) were found in the asymmetric unit and refined. The attribution of the space group was made

Table 3. Crystal Data and Structure Refinement Details for 2 and 3

	2	3
empirical formula	$C_{20}H_{22}Cl_2N_2Ti$	$C_{62}H_{74}Cl_2N_8Zr_2$
fw	409.20	1184.63
cryst syst	triclinic	monoclinic
space group	$P\bar{1}$	$P2_1$
unit cell dimens	$a = 7.211(2)$ Å	$a = 12.505(2)$ Å
	$b = 10.872(2)$ Å	$b = 15.839(3)$ Å
	$c = 14.069(2)$ Å	$c = 17.342(3)$ Å
	$\alpha = 98.41(2)$ deg.	
	$\beta = 102.31(2)$ deg	$\beta = 90.113(1)$ deg
	$\gamma = 106.73(2)$ deg	
volume	1006.4(4) Å^3	3434.9(9) Å^3
Z	2	2
calcd density	1.350 Mg/m^3	1.145 Mg/m^3
abs coeff	0.695 mm^{-1}	0.420 mm^{-1}
$F(000)$	424	1232
Flack param		−0.04(6)
no. of reflns	4160/3939	7288/6961
no. collected/unique	[R(int) = 0.0262]	[R(int) = 0.0158]
completeness to $\theta = 26.03°$	99.3%	99.5%
no. of data/restraints/params	3939/0/226	6961/1/663
goodness-of-fit on F^2	1.052	1.035
final R indices [$I > 2\sigma(I)$]	$R_1 = 0.0611$	$R_1 = 0.0525$
	$wR_2 = 0.1404$	$wR_2 = 0.1262$
R indices (all data)	$R_1 = 0.1054$	$R_1 = 0.0760$
	$wR_2 = 0.1674$	$wR_2 = 0.1373$
largest diff peak and hole	0.449 and −0.438 e Å^{-3}	0.591 and −0.384 e Å^{-3}

unambiguously, the data being acentric. For both complexes all non-hydrogen atoms were refined anisotropically, and the hydrogen atoms were inserted in idealized positions riding on the parent C atom. Figures were made with ORTEP3.[25]

Data were deposited in the CCDC under the deposit numbers CCDC 205751 for **2** and CCDC 205752 for **3**.

Computational Details. The geometry optimizations were accomplished by means of ab initio and DFT calculations performed with the Gaussian 98 program.[26] The B3LYP hybrid functional was used in all optimizations. That functional includes a mixture of Hartree−Fock[9] exchange with DFT[10] exchange−correlation, given by Becke's three-parameter functional[27] with the Lee, Yang, and Parr correlation functional, which includes both local and nonlocal terms.[28] All the optimized geometries are the result of full optimizations without any symmetry constraints. The calculations were performed on model complexes with the substituents of the coordinated amido (NR_2), R, and the entering isonitriles (CNR′), R′, replaced by hydrogen atoms (R = R′ = H) in all cases except for the two addition steps (Figure 4a and c). In these cases, a methyl substituent was used for the amido ligands (R = Me), since with R = H the transition state search was masked by an artificial hydrogen interaction between the incoming isonitrile carbon and the coordinated amido, NH···CNH. Computational limitations prevented us from using R = Me in all calculations.

The basis set used for the geometry optimizations (B1) consisted of a standard 3-21G(*)[29] with a d-polarization function added for Cl[30] and an f-polarization function added for the metal atoms.[31] Transition state optimizations were performed with the synchronous transit-guided quasi-Newton method (STQN) developed by Schlegel et al.[32] All stationary points were confirmed by frequency calculations. Single-point energy calculations were run on the optimized structures at the same theory level and a basis set (B2) that consisted of the previous one for Zr and a standard 6-31G*[33] for the remaining elements (Ti, C, H, N, and Cl). The energies were zero-point corrected with the zero-point energies obtained at the B3LYP/B1 level.

A natural population analysis (NPA)[34] was performed in order to evaluate the charge distribution on the optimized complexes, and the Wiberg indexes (WI)[35] obtained are used as a measure of bond strength.

Acknowledgment. This work was supported by Fundação para a Ciência e a Tecnologia, Portugal (PBICT/P/QUI/2163/95). S.S.R. is grateful for a FCT scholarship.

Supporting Information Available: Tables of atomic coordinates for all the optimized structures. This material is available free of charge via the Internet at http://pubs.acs.org.

OM030211N

(22) Altomare, A.; Burla, M. C.; Camalli, M.; Cascarano, G.; Giacovazzo, C.; Guagliardi, A.; Moliterni, A. G. G.; Polidori, G.; Spagna, R. Sir97: A new tool for crystal structure determination and refinement. *J. Appl. Crystallogr.* **1998**, *32*, 115.

(23) Sheldrick, G. M. *SHELXL-97*: A program for refining crystal structures; University of Göttingen: Germany, 1997.

(24) Farrugia, L. J. WingX (v1.64.03b). *J. Appl. Crystallogr.* **1999**, *32*, 837.

(25) Farrugia, L. J. *J. Appl. Crystallogr.* **1997**, *30*, 565.

(26) Frisch, M. J.; Trucks, G. W.; Schlegel, H. B.; Scuseria, G. E.; Robb, M. A.; Cheeseman, J. R.; Zakrzewski, V. G.; Montgomery, J. A., Jr.; Stratmann, R. E.; Burant, J. C.; Dapprich, S.; Millam, J. M.; Daniels, A. D.; Kudin, K. N.; Strain, M. C.; Farkas, O.; Tomasi, J.; Barone, V.; Cossi, M.; Cammi, R.; Mennucci, B.; Pomelli, C.; Adamo, C.; Clifford, S.; Ochterski, J.; Petersson, G. A.; Ayala, P. Y.; Cui, Q.; Morokuma, K.; Malick, D. K.; Rabuck, A. D.; Raghavachari, K.; Foresman, J. B.; Cioslowski, J.; Ortiz, J. V.; Stefanov, B. B.; Liu, G.; Liashenko, A.; Piskorz, P.; Komaromi, I.; Gomperts, R.; Martin, R. L.; Fox, D. J.; Keith, T.; Al-Laham, M. A.; Peng, C. Y.; Nanayakkara, A.; Gonzalez, C.; Challacombe, M.; Gill, P. M. W.; Johnson, B.; Chen, W.; Wong, M. W.; Andres, J. L.; Gonzalez, C.; Head-Gordon, M.; Replogle, E. S.; Pople, J. A. *Gaussian 98*, Revision A.6; Gaussian, Inc.: Pittsburgh, PA, 1998.

(27) Becke, A. D. *J. Chem. Phys.* **1993**, *98*, 5648.

(28) (a) Lee, C.; Yang, W.; Parr, R. G. *Phys. Rev. B* **1988**, *37*, 785. (b) Miehlich, B.; Savin, A.; Stoll, H.; Preuss, H. *Chem. Phys. Lett.* **1989**, *157*, 200.

(29) (a) Binkley, J. S.; Pople, J. A.; Hehre, W. J. *J. Am. Chem. Soc.* **1980**, *102*, 939. (b) Gordon, M. S.; Binkley, J. S.; Pople, J. A.; Pietro, W. J.; Hehre, W. J. *J. Am. Chem. Soc.* **1982**, *10*, 2797. (c) Pietro, W. J.; Francl, M. M.; Hehre, W. J.; Defrees, D. J.; Pople, J. A.; Binkley, J. S. *J. Am. Chem. Soc.* **1982**, *104*, 5039. (c) Dobbs, K. D.; Hehre, W. J. *J. Comput. Chem.* **1986**, *7*, 359. (d) Dobbs, K. D.; Hehre, W. J. *J. Comput. Chem.* **1987**, *8*, 861. (e) Dobbs, K. D.; Hehre, W. J. *J. Comput. Chem.* **1987**, *8*, 880.

(30) Höllwarth, A.; Böhme, M.; Dapprich, S.; Ehlers, A. W.; Gobbi, A.; Jonas, V.; Köhler, K. F.; Stegmann, R.; Veldkamp, A.; Frenking, G. *Chem. Phys. Lett.* **1993**, *208*, 237.

(31) Ehlers, A. W.; Böhme, M.; Dapprich, S.; Gobbi, A.; Höllwarth, A.; Jonas, V.; Köhler, K. F.; Stegmann, R.; Veldkamp A.; Frenking, G. *Chem. Phys. Lett.* **1993**, *208*, 111.

(32) (a) Peng, C.; Ayala, P. Y.; Schlegel, H. B.; Frisch, M. J. *J. Comput. Chem.* **1996**, *17*, 49. (b) Peng, C.; Schlegel, H. B. *Isr. J. Chem.* **1994**, *33*, 449.

(33) (a) Ditchfield, R.; Hehre W. J.; Pople, J. A. *J. Chem. Phys.* **1971**, *54*, 724. (b) Hehre, W. J.; Ditchfield R.; Pople, J. A. *J. Chem. Phys.* **1972**, *56*, 2257. (c) Hariharan, P. C.; Pople, J. A. *Mol. Phys.* **1974**, *27*, 209. (d) Gordon, M. S. *Chem. Phys. Lett.* **1980**, *76*, 163. (e) Hariharan, P. C.; Pople, J. A. *Theor. Chim. Acta* **1973**, *28*, 213.

(34) (a) Carpenter, J. E.; Weinhold, F. *J. Mol. Struct. (THEOCHEM)* **1988**, *169*, 41. (b) Carpenter, J. E. Ph.D. Thesis, University of Wisconsin: Madison, WI, 1987. (c) Foster, J. P.; Weinhold, F. *J. Am. Chem. Soc.* **1980**, *102*, 7211. (d) Reed, A. E.; Weinhold, F. *J. Chem. Phys.* **1983**, *78*, 4066. (e) Reed, A. E.; Weinhold, F. *J. Chem. Phys.* **1983**, *78*, 1736. (f) Reed, A. E.; Weinstock, R. B.; Weinhold, F. *J. Chem. Phys.* **1985**, *83*, 735. (g) Reed, A. E.; Curtiss, L. A.; Weinhold, F. *Chem. Rev.* **1988**, *88*, 899. (h) Weinhold, F.; Carpenter, J. E. *The Structure of Small Molecules and Ions*; Plenum: New York, 1988; p 227.

(35) Wiberg, K. B. *Tetrahedron* **1968**, *24*, 1083.